16th World Conference on Earthquake, 16WCEE 2017
Santiago Chile, January 9th to 13th 2017
Paper N° 2571
Registration Code: S-W1463099704

TRIAXIAL MATERIAL MODEL FOR CONCRETE STRUCTURES UNDER CYCLIC LOADING

M. Moharrami(1), I. Koutromanos(2)

(1) *Graduate Student, Department of Civil and Environmental Engineering, Virginia Polytechnic Institute and State University, mrmg@vt.edu*
(2) *Assistant Professor, Department of Civil and Environmental Engineering , Virginia Polytechnic Institute and State University, ikoutrom@vt.edu*

Abstract

This paper presents the formulation of a material model for the analysis of concrete under multiaxial, cyclic loading conditions, and its use for the analysis of failure of reinforced concrete structures. The model combines an elastoplastic formulation with a non-associative flow rule to capture compression-dominated behavior and a rotating smeared-crack model to capture the tension-dominated behavior. The proposed formulation resolves the issues which exist in many available concrete material models, related to properly capturing the crack opening and closing behavior and accounting for the effect of confinement on the strength and ductility under compression-dominated stress states. The concrete material model is combined with a constitutive model for reinforcing steel which can account for the hysteretic response and for the material failure due to low-cycle fatigue. Validation analyses for reinforced concrete components show that the analytical models can capture the damage patterns and the hysteretic response.

Keywords: Triaxial Constitutive model; Concrete structures; Cyclic loading; Confinement effect; Rebar Buckling and Rupture;

1. Introduction

Reinforced concrete (RC) structures constitute a significant portion of the building inventory in earthquake-prone regions. The quantitative evaluation of the performance of such structures to extreme loading events such as earthquakes is instrumental for characterizing the safety and resilience of built communities. Cyclic loading induced by earthquakes leads to the formation of cracks in the concrete. Additionally, significant compressive strains are expected to occur in, e.g., the compression zone of the inelastic hinge regions in flexural members such as beams or columns. Modern design standards stipulate that, for structures located in regions with high seismicity, inelastic deformability of the concrete under compression must be ensured by means of transverse reinforcement which leads to the development of a confining pressure. This confinement effect has been found to lead to an increase in the compressive strength and ductility of concrete (e.g., [1],[2]).

Typically, the analysis of RC structures such as frames and walls is conducted with models based on uniaxial stress-strain laws. Such models are numerically efficient and allow systematic parametric investigations, but they inherently lack the capability to accurately describe the behavior of regions like beam-to-column joints, shear keys etc., where multiaxial stress states may develop in the concrete. Additionally, the effect of confinement contributed by the transverse reinforcement is accounted for in these models in a simplified fashion, i.e. by a prior adjustment of the parameters of the uniaxial material laws using simplified equations (e.g., [1]). The only means to accurately determine the behavior of regions where multiaxial stress states develop is to use continuum-based finite element analyses with appropriate constitutive models which can capture the interaction of the various stress and strain components.

A number of triaxial constitutive models ([2]-[11]) have been formulated and proposed for concrete. As explained in a recent study by Moharrami and Koutromanos [12], these models have either been limited to monotonic loading conditions, have been unable to accurately capture all aspects of material response, or have been characterized by inability of the stress update algorithms to converge. Given the issues pertaining to available multiaxial constitutive models for concrete, a sufficiently accurate and numerically efficient material model to allow the analysis of RC components under cyclic loading is much needed. The present paper describes the formulation of a material model for the analysis of RC structures, with an emphasis to analysis under earthquake loads. The model has been combined with a recently developed material law for reinforcing steel which can capture the hysteretic response and rupture due to low-cycle fatigue. Validation analyses are conducted for reinforced concrete components subjected to cyclic loads and incurring severe damage in the form of cover loss, rebar buckling and subsequent rebar rupture.

2 Description of Model

The model described herein can capture all the aspects of behavior, such as compressive crushing, strength and stiffness degradation due to cracking, and the effect of confinement on the material strength and ductility. The strain vector is essentially decomposed into three parts, namely an elastic part, a plastic part and a cracking part. The plastic part is to capture inelastic strains associated with compressive stresses. A detailed description of the model formulation is provided in [12]. The same reference presents parametric analyses elucidating the effect of mesh size, the need for adjusting (regularizing) the compressive softening law with element size and the impact of alternative yield surfaces on the obtained results. An overview of the salient features of the material model is provided here for completeness.

2.1.1 Elastoplastic Model for Uncracked Material

The behavior of the uncracked material is governed by an elastoplastic constitutive model. The formulation is established in total form, in accordance with the following equation.

$$\{\sigma\} = [D]\{\varepsilon^{el}\} = [D]\left(\{\varepsilon\} - \{\varepsilon^{pl}\} - \{\varepsilon^{cr}\}\right) \tag{1}$$

In Eq. (1), $\{\sigma\}$ is the stress vector, $\{\varepsilon^{el}\}$ is the elastic strain vector, and $\{\varepsilon\}$, $\{\varepsilon^{pl}\}$, $\{\varepsilon^{cr}\}$ are the total, plastic, and cracking strain vector, respectively. The stress-strain law can be formulated in the principal stress-strain space as follows.

$$\{\hat{\sigma}\} = [\hat{D}]\{\hat{\varepsilon}^{el}\} \tag{2}$$

where $\{\hat{\sigma}\}$ and $\{\hat{\varepsilon}^{el}\}$ are column vectors containing the principal stresses and principal elastic strains, respectively. Assuming that the elastic stiffness matrix, $[\hat{D}]$, is that of an isotropic material, its components can be expressed in terms of the elastic modulus, E, and Poisson's ratio, v, as follows.

$$[\hat{D}] = \frac{E}{(1+v)(1-2v)}\begin{bmatrix} 1-v & v & v \\ v & 1-v & v \\ v & v & 1-v \end{bmatrix} \tag{3}$$

The yield surface in the principal stress space is described by the following equation.

$$f\left(\{\hat{\sigma}\},\kappa\right) = \frac{1}{1-\alpha}\left[\alpha \cdot I_1 + r(\theta,e)\sqrt{3J_2}\right] - c_c(\kappa) = 0 \tag{4}$$

Parameters I_1 and J_2 in Eq. (4) are the first invariant and second deviatoric invariant, respectively, of the stress tensor, c_c is a strength parameter which can be shown to be equal to the uniaxial compressive strength, κ is a hardening parameter expressing the cumulative effect of inelastic deformation, α is a material parameter, and $r(\theta,e)$ is a radial distance which itself is a function of eccentricity, e, and the Lode angle, θ, as explained in Kang et al. [13]. The shape of the yield surface on the deviatoric plane as compared to the well-known Drucker-Prager surface is shown in Fig. 1a. The proposed yield surface is inscribed to the Drucker-Prager one. It is worth mentioning that, as the confining pressure increases, the two surfaces become more and more similar.

The growth rate of the plastic strains was defined using the following equation. The value of α can be determined from the following expression ([14]).

$$\alpha = \frac{f_b - f_c}{2f_b - f_c} \tag{5}$$

where f_c is the uniaxial compressive strength of the material and f_b is the biaxial compressive strength.

A rate equation is established for the evolution of the plastic strains. Specifically, each component of the plastic strain rate tensor is obtained by multiplying a scalar plastic multiplier, $\dot{\lambda}$, with the partial derivative of a plastic potential function, g, with respect to the corresponding component of the stress tensor.

$$\dot{\varepsilon}_{ij}^{pl} = \dot{\lambda}\frac{\partial g}{\partial \sigma_{ij}} \tag{6}$$

The plastic potential function for the present model is described by the following equation.

$$g = \alpha_p \cdot I_1 + \sqrt{2J_2} \tag{7}$$

where α_p is a dilatancy parameter, controlling the volumetric expansion of the material due to inelastic behavior. Differentiating Eq. (7) with respect to the stress components gives:

$$\frac{\partial g}{\partial \sigma_{ij}} = m_{ij} = \alpha_p \delta_{ij} + \frac{s_{ij}}{\sqrt{2J_2}} \tag{8}$$

where δ_{ij} is the Kronecker delta and s_{ij} is the ij-component of the deviatoric stress tensor.

The material model is preferably formulated in terms of the principal stresses, at which case the following equation is obtained for each of the three principal directions of the rate of plastic strain.

$$\dot{\hat{\varepsilon}}_i^{pl} = \dot{\lambda}\left(\alpha_p + \frac{\hat{s}_i}{\sqrt{2J_2}}\right),\ i = 1,2,3 \tag{9}$$

The strength of the material changes with the accumulation of inelastic strains in accordance with the following hardening-softening law, originally used in [7].

$$c_c(\kappa) = \frac{f_o}{a}\left[(1+a)\sqrt{\varphi(\kappa)} - \varphi(\kappa)\right] \geq f_{res} \tag{10}$$

where f_{res} is the residual compressive strength in the material, κ is a non-negative hardening variable which is initially equal to zero, f_o and a are material constants, and φ(κ) is an increasing function given by the following equation:

$$\varphi(\kappa) = 1 + a(2+a)\kappa \tag{11}$$

The evolution of κ is governed by the following rate equation, which is an enhanced version of that formulated by Lee and Fenves in [7].

$$\dot{\kappa} = \frac{c_c}{g_c} \cdot \left.\frac{\partial g}{\partial \hat{\sigma}}\right|_{\hat{\sigma}_{min}} \cdot e^{d(1+X)\frac{p}{f_c}} \tag{12}$$

where g_c is a material parameter giving the area under the plot of the hardening-softening law and $\left.\frac{\partial g}{\partial \hat{\sigma}}\right|_{\hat{\sigma}_{min}}$ is the component of the rate of plastic strain vector in the direction of the minimum principal stress. The exponential term, for which factor d is a user-defined constant, expresses the effect of pressure on the evolution of the hardening variable. The pressure, p, is related to the first invariant of the stress tensor.

$$p = -\frac{I_1}{3} \tag{13}$$

The greater the pressure value, the greater the confinement effect on the material. The parameter X in Eq. (12) is given from the following expression.

$$X = \frac{I_1}{\sqrt{3J_2}} \tag{14}$$

The exponential term in Eq. (12) is equal to 1 for uniaxial compression and it decreases for multiaxial compressive states, meaning that the evolution of the hardening-softening variable becomes slower for the case of multiaxial compressive states. In this fashion, the exponential term, which was not present in the model by Lee and Fenves [7], accounts for the increased ductility of confined concrete. In the limit, the value of X becomes minus infinity for isotropic compression, meaning that there is no evolution in the hardening variable. Of course, the case of isotropic compression cannot practically occur in the computation of X since isotropic compression stress states are always purely elastic states in the proposed model.

The variation of the strength parameter c_c with κ is presented in Fig. 1b. It is worth mentioning that the maximum value of $c_c = f_c$ is obtained for $\kappa = \kappa_o$, where κ_o is the value of κ which gives a zero first derivative of c_c. In the analyses presented herein, f_o is set equal to $0.66f_c$. The values of κ_o and "a" can be found if the strain ε_o at the peak compressive strength and the area g_c under the plot of the hardening-softening law are given, as explained in [12]. The parameter g_c can be obtained by stipulating that the area under the softening portion of the hardening law is equal to the ratio G_c/h, where G_c is a compressive fracture energy of the material and h is a mesh size parameter for the finite element model. Lubliner et al. [14] have argued that G_c cannot be identified with a particular physical energy. Despite such objections pertaining to the existence of a compressive fracture energy, the value of G_c is established in the present study as follows. First, an empirical equation by Bazant [15], providing the best fit to a large number of data sets, is used to calculate the tensile (mode-1) fracture energy, G_t, of the material. Then, G_c is obtained by multiplying G_t by 100.

2.2 Rotating Crack Model for Cracked Material

If the cracking criterion is met in one of the principal directions – i.e., the stress in that direction is greater than the cracking strength of the material, then the stress must be corrected to account for the currently active crack. The principal stress of the cracked material is a function of the corresponding principal cracking strain in accordance with the following equation.

$$\hat{\sigma}_i = c_t \cdot \left[(1-M) e^{-\lambda_t \frac{\hat{\varepsilon}_i^{cr} - \hat{\varepsilon}_{ini}}{f_t}} + M \right] \tag{15}$$

where M is the fraction of residual tensile strength, $\hat{\varepsilon}_{ini}$ is the strain at onset of softening and λ_t is a parameter controlling the rate of tensile softening. The value of material tensile strength, c_t, is obtained by the following expression.

$$\begin{aligned} c_t &= f_t, \text{ if } \kappa \le \kappa_o \\ c_t &= \frac{c_c}{f_c} f_t, \text{ if } \kappa > \kappa_o \end{aligned} \tag{16}$$

Equation (16) implies that, if the material has reached the stage of compressive strength degradation, then the tensile strength will be subjected to a similar reduction. For unreinforced concrete, the value of parameter λ_t is obtained by stipulating that the area under the softening portion of the cracking stress-strain law is equal to the ratio G_t/h, where G_t is the tensile (mode-I) fracture energy of the material. For reinforced concrete, the values of M and λ_t can be found using, e.g., the approach given by Lu and Panagiotou [16] which accounts for the tension stiffening effect of the reinforcement. The softening law of the cracked material and the unloading-reloading behavior in the cracked regime are schematically presented in Fig. 1c.

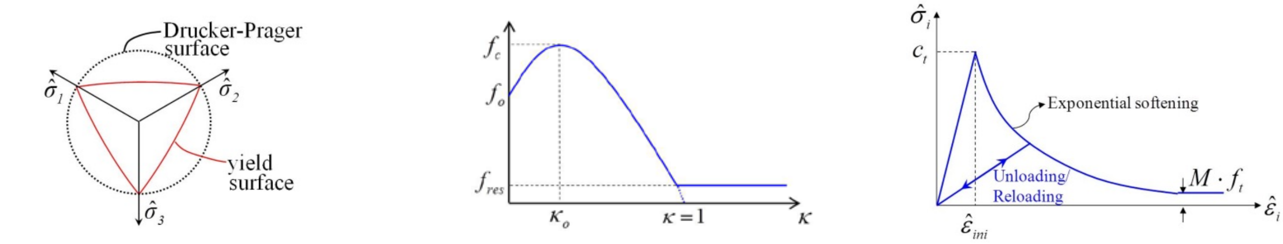

(a) Yield surface on deviatoric plane (b) Hardening-softening law (b) Crack Model

Fig. 1 – Yield Surface and Hardening-softening law for elastoplastic model and crack stress-strain model

The behavior of the model at the material level is validated with single-element analyses. A first analysis is used to determine the performance of the model for cyclic loading in the tensile regime. To this end, the results of the experimental test by Gopalaratnam and Shah [17] are compared to the corresponding results obtained with the proposed model in Fig. 2a. Additional single-element analyses are conducted to demonstrate the behavior of the material under confined compression. Single-element analyses are performed for monotonically increasing compression, under different levels of confining pressure, and the results are presented in Fig. 2b. To allow the calibration of the dimensionless parameter d, which expresses the effect of confinement on material ductility, the analyses have also been conducted using the model by Maekawa et al. [8], which has been shown to be capable of capturing the increased material strength and ductility due to confinement. The single-element analyses demonstrate that the proposed model can satisfactorily capture the cyclic crack opening and closing and the effect of confinement on the strength and ductility of the material.

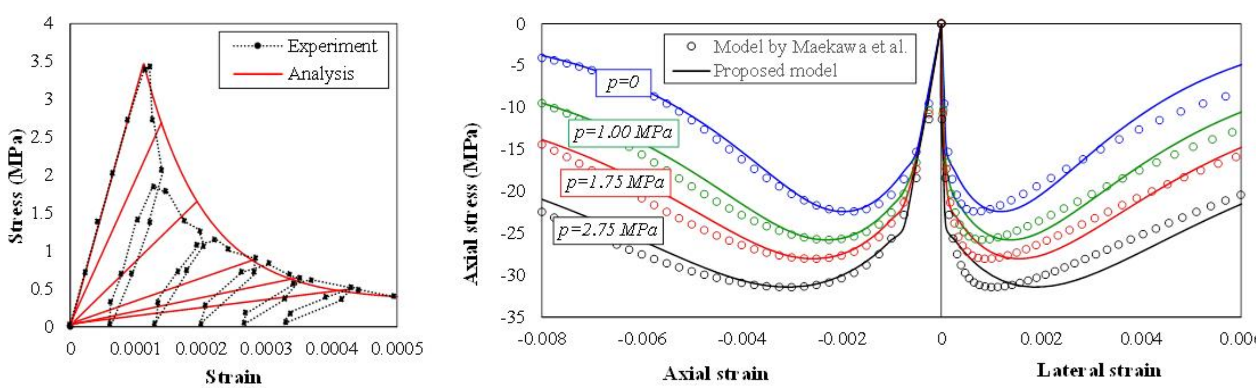

(a) Cyclic tensile loading (b) Behavior for confined compression

Fig. 2 - Single element analysis results

3 Analysis of RC components under cyclic loading

The proposed model has been implemented in the commercial finite element program LS-DYNA [18] to allow the simulation of structural components and systems under cyclic loading. An explicit transient integration scheme is employed for the solution of the global equations in the models. Specifically, the global equations are formulated as a dynamic problem, and a central-difference scheme is employed for integration of the global response in time. In general, implicit static solution algorithms may be deemed preferable for quasi-static loading, because they eliminate the possibility for spurious inertial effects on the solution. However, such algorithms typically entail large memory requirements (due to the need to store a global tangent stiffness matrix). Furthermore, implicit schemes may not be appropriate for simulations of failure or collapse, due to the probability of failure of the global solution algorithms to converge.

In the analytical models, the concrete is represented with three-dimensional, hexahedral solid elements, having a uniform reduced integration (URI), i.e., a single quadrature point. While URI enhances the efficiency of finite element formulations, by substantially reducing the computational cost stemming from the stress update at the quadrature points of the mesh, it also entails the presence of spurious zero-energy modes (hourglass modes), for which URI-based elements cannot develop resistance. For this reason, hourglass control is used in the analyses presented herein, to prevent spurious zero-energy modes from polluting the obtained analytical results. The stress-strain response of the solid elements is described by the constitutive model proposed herein, and the calibration of the material parameters for the concrete model is summarized in Table 1.

In the analyses, the material response of the steel reinforcement is described by the formulation by Kim and Koutromanos [19], which is essentially an enhanced version of the material model by Dodd and Restrepo [20], eliminating the need for an iterative stress update algorithm and also accounting for rupture due to low-cycle fatigue. The material model includes appropriate laws to capture the monotonic and cyclic uniaxial response of reinforcing steel, as shown in Figs. 3a and 3b, respectively. The specific material law only requires knowledge of the monotonic tensile response of reinforcement to calibrate all the parameters. The values of the steel model parameters for the validation analyses are provided in Table 2. In accordance with Fig. 3a, E_s is the steel modulus of elasticity, f_y is the yield stress, ε_{sh} is the strain at onset of strain hardening, ε_{sh1} and f_{sh1} are the strain and stress, respectively, at an intermediate point lying on the hardening portion of the monotonic curve, f_u is the ultimate strength and ε_u is the corresponding ultimate strain. The reinforcing bars are simulated with corotational beam elements. This allows to inherently account for the effect of inelastic rebar buckling, without a need to define initial imperfection on the beam elements, as also described in [8]. The effect of strain penetration at the base of the RC components is also accounted for, by introducing one-dimensional contact elements between the rebar elements and the surrounding solid elements representing the concrete. The traction-separation law of the contact elements is defined along the axial direction of the rebars, and it essentially is a simplified form of the bond-slip law of Murcia-Delso et al. [21].

Finally, the models employ element removal to capture the loss of cover concrete and the fracture of reinforcing steel bars due to low-cycle fatigue.

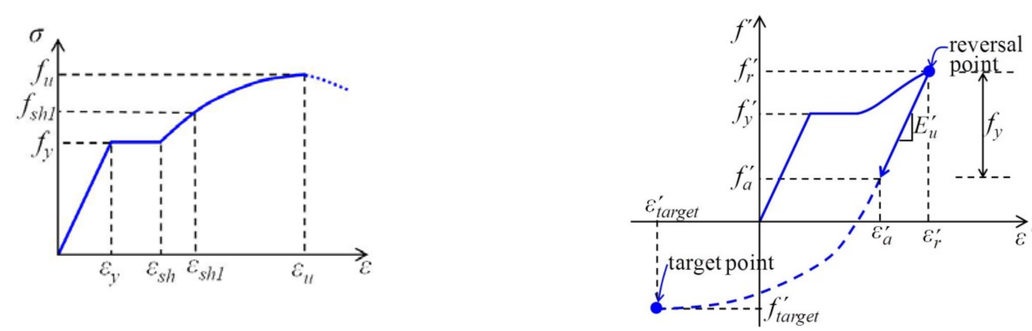

(a) Monotonic Tensile Response (b) Cyclic Hysteretic Response

Fig. 3 – Behavior of Reinforcing steel Model (figures from [19])

Table 1 – Calibration of Concrete Model Parameters for Structural Components

Specimen	f_c (MPa)	ε_o	a_p	a	d	G_t (N/m)	G_c (N/m)	M
Beyer et al. [20]	77.9	0.0025	0.15	0.375	11.0	108.9	11980	0.025
Schoettler et al. [21]	41.3	0.0025	0.15	0.375	6.0	83.6	9193	0.036

Table 2 – Calibration of Reinforcing Steel Material Model Parameters for Structural Components

Specimen	Bar	E_s (MPa)	f_y (MPa)	ε_{sh}	ε_{sh1}	f_{sh1} (MPa)	ε_u	f_u (MPa)
Beyer et al. [22]	#2	200000	518	0.004	0.04	650	0.084	681
	#4	200000	488	0.025	0.06	550	0.126	595
Schoettler et al. [23]	#11	195990	518.5	0.011	0.04	606.7	0.11	706
	#5	200000	377.8	0.002	0.04	517	0.125	592.2

3.1 Analysis of U-shaped reinforced concrete wall under bi-directional quasi-static cyclic loading

The first analysis presented herein is conducted for a U-shaped RC wall specimen tested by Beyer et al. [22] and referred to therein as specimen TUA. The specimen was subjected to bi-directional cyclic lateral loading until the occurrence of severe strength and stiffness degradation due to rebar rupture and concrete crushing.

As shown in Fig. 4a and 4b, the height of the specimen was 2.65 meters (104 in), and the thickness of the wall was equal to 150 mm (5.9 in). The boundary regions of the wall section included twenty-two longitudinal bars with diameter of 12 mm (#4 bars) while the web portion of the wall section included a total of twenty-eight rebars with a diameter of 6 mm (#2 bars). The transverse reinforcement at the wall boundaries consisted of transverse ties with a diameter of 6 mm and a 50-mm spacing, while the web regions of the wall section included transverse bars with a diameter of 6 mm and a spacing of 125 mm (4.9 in). The specimen was restrained against rotation at the base and subjected to prescribed cyclic bi-directional displacement history. The displacement histories were applied at a height of 2.95 m (116 in) and 3.35 m (132 in) for loading in the X and Y direction, respectively.

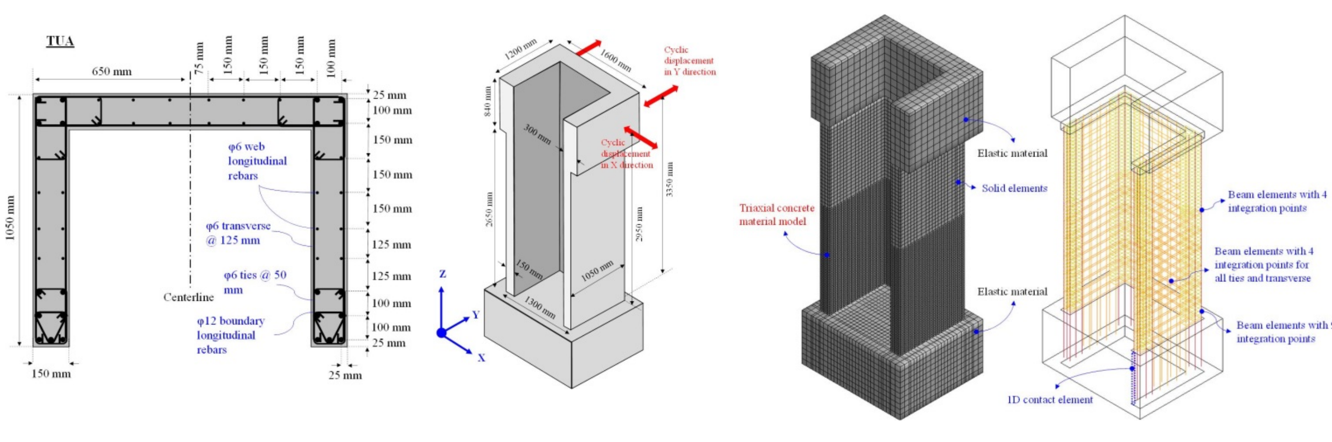

a) Plan View b) Isometric View c) Computational Model

Fig. 4 - Configuration and computational model of RC wall tested by Beyer et al. [22]

The finite element model of the wall specimen is depicted in Fig. 4c. Since the model used an explicit dynamic time-marching scheme to simulate quasi-static loading. For this reason, special care was taken (by applying the prescribed displacements at a very slow rate) to ensure that the analytical solution would not be affected by dynamic effects. The analytically obtained hysteretic response of the specimen is compared to the corresponding experimental observations in Fig. 5. As can be seen from Fig. 5, both the maximum strength and the initial stiffness of the specimen is well predicted in Y direction, and they are only slightly underestimated for the X direction. The analysis also provides a satisfactory representation of the hysteretic response of the specimen.

In both the analytical model and the experimental test, severe damage occurred due to rebar fracture, as shown in Fig. 6. Similar to the experiment, the first rebar rupture in the analysis occurred during the first loading cycle with a drift ratio of 2.5% along the X direction. Additionally, the analytical model successfully captured the damage associated with cover spalling and flexural and shear cracking in the specimen, as depicted in Fig. 7.

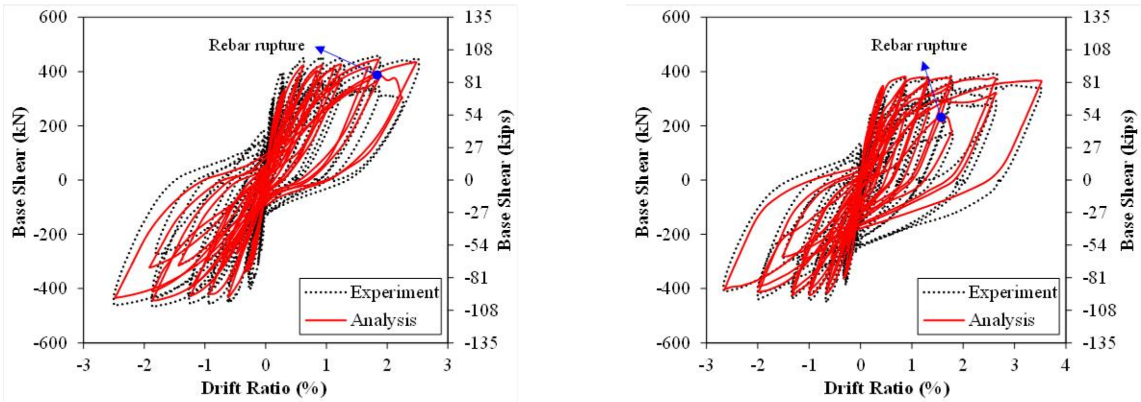

(a) X-direction (b) Y-direction

Fig. 5 – Comparison of analytically obtained and experimentally recorded hysteretic response for the RC wall specimen tested by Beyer et al. [22].

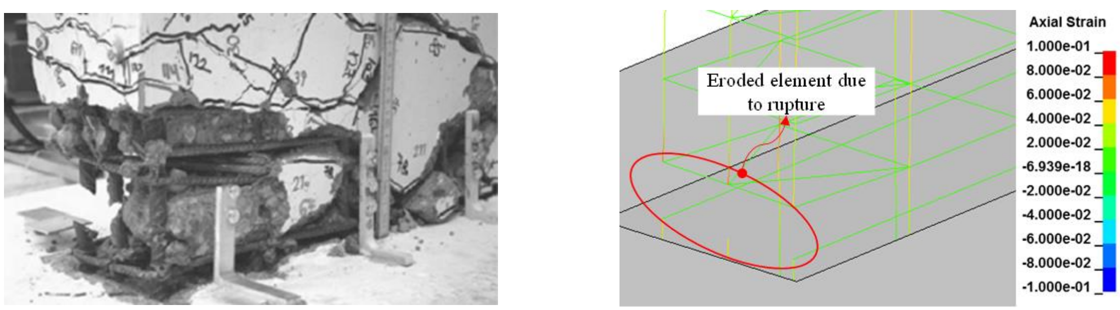

(a) Experiment (picture from [22]) (b) Analysis

Fig. 6 - Rebar rupture in the U-shaped wall tested by Beyer et al. [22].

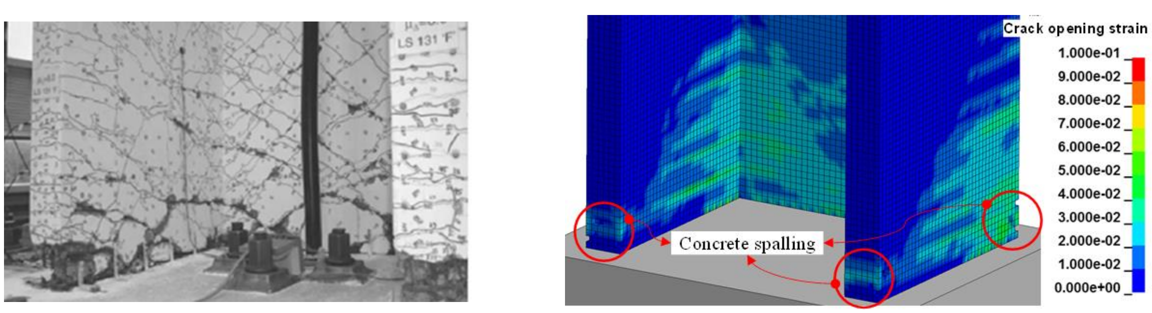

(a) Experiment (picture from [22]) (b) Analysis

Fig. 7 - Cover spalling and cracking in the U-shaped wall tested by Beyer et al. [22].

3.2 Analysis of a full-scale reinforced concrete bridge pier subjected to seismic loading

Analysis is also conducted for a full-scale, reinforced concrete, bridge column tested by Schoettler et al. [23]. The column was designed based on modern seismic provisions and subjected to the sequence of ten ground motions. The column had a height of 7.31 m (288 in) and a circular cross-section with a diameter of 1.22 m (48 in) with eighteen #11 vertical rebars. The transverse reinforcement consisted of double #5 ties at a spacing of 152 mm (6 in). The column configuration and reinforcing details are depicted in Fig. 8a. The specimen was restrained against rotation at the bottom of the footing, and a concrete block with a total weight of 2.32 MN (521 kips) was added on top of the specimen to represent the seismic mass. The finite element model of the specimen is presented in Fig. 8b and has been analyzed for the entire motion sequence of the specimen.

A finite element model including solid elements for concrete, beam elements for reinforcement, and 1D contact elements to account for bond-slip, is developed for the column as depicted schematically in Fig. 8b. The analysis is conducted for the entire motion sequence applied on the specimen.

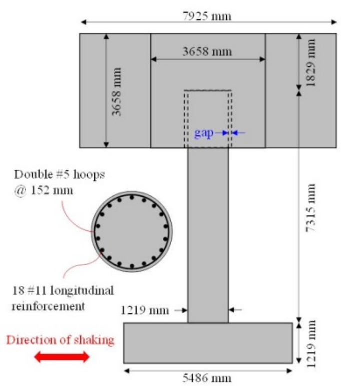

(a) Dimensions and reinforcement detail

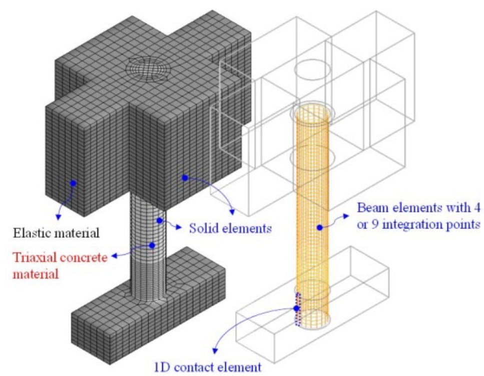

(b) Finite element model

Fig. 8 - Configuration and analytical model for the column tested by Schoettler et al. [23].

The analytically obtained drift time histories for nine out of the ten motions of the sequence are compared to the corresponding experimental records in Fig. 9. A very good agreement is obtained in terms of predicting the peak displacements and drift histories, except for the last motion in the sequence. During the experimental test for that motion, the column came to contact with a safety support tower that was provided to prevent damage on the shake table from total collapse of the specimen. Since the effect of this support tower is not accounted for in the analytical model, a discrepancy between analysis and experiment is expected for this motion.

Similarly to the experimental test, the analytical model predicts that first yield of the longitudinal reinforcement occurs during the third ground motion. During the same motion, concrete cover spalling is observed for the first time in the analytical model, as depicted in Fig. 10a. During the fifth and sixth motions, more extensive loss of cover material occurred in the test, and more cover elements are removed in the analysis, as shown in Fig. 10b. At the end of the sixth motion, the core concrete in the vicinity of the base of the column was significantly damaged, as shown in Fig. 11. The experimental test specimen eventually incurred significant damage in the form of rebar buckling and subsequent rupture, as shown in Fig. 12a. In the analytical model, the buckling of rebars is visually observed during the seventh motion, similar to the corresponding experimental observation, and it is significant during the eighth motion, as shown in Fig. 12b. Additionally, as depicted in Fig. 12c, the first rebar rupture is obtained during the eighth ground motion, which was also the case for the experimental test.

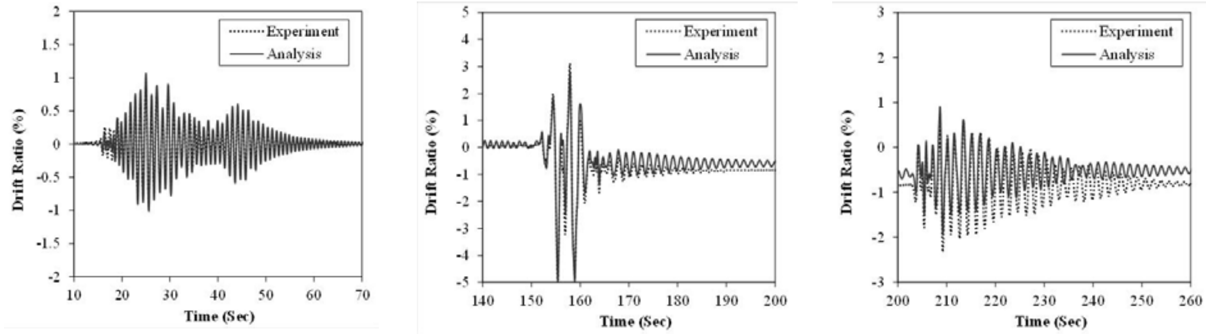

(c) EQ2: 100% Loma Prieta-90° (d) EQ3: 100% Loma Prieta (e) EQ4: 100% Loma Prieta-90°

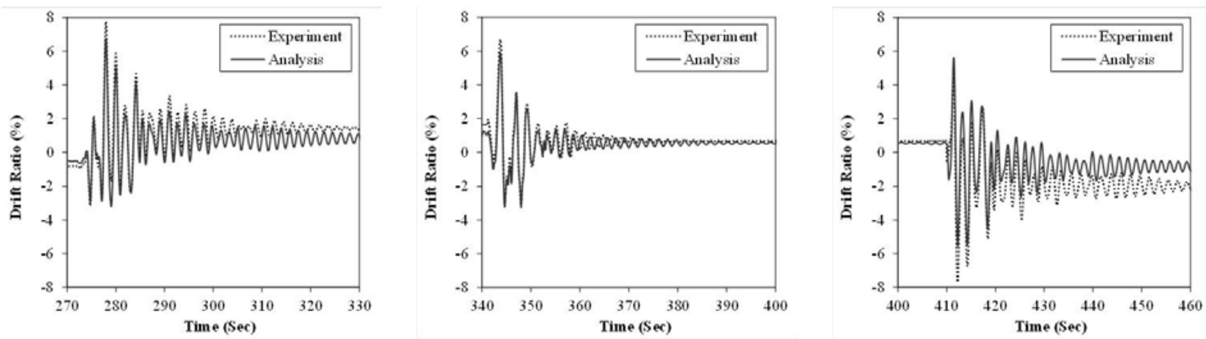

(f) EQ5: 100% Kobe (g) EQ6: 100% Loma Prieta (h) EQ7: 100% Kobe

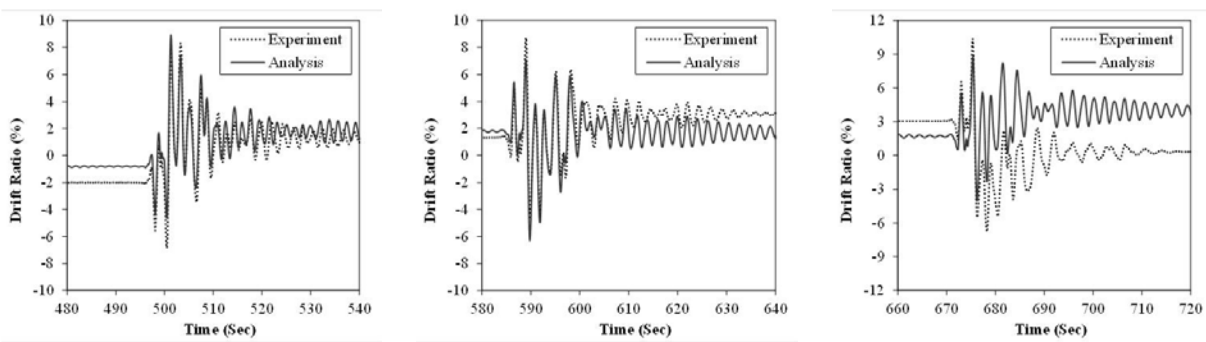

(i) EQ8: -120% Kobe (j) EQ9: 120% Kobe (k) EQ10: 120% Kobe

Fig. 9 - Comparison of analytically obtained and experimentally recorded drift histories for the column tested by Schoettler et al. [23].

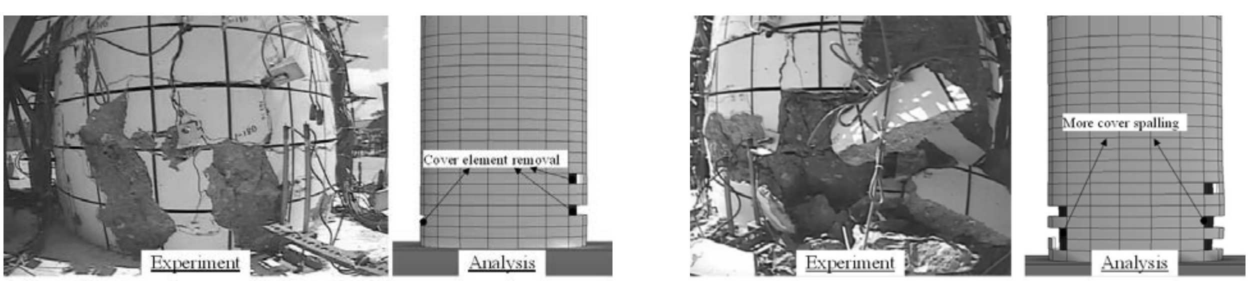

a) After the third motion (test picture from [23]) b) After the fifth motion (test picture from [23])

Fig. 10 - Loss of cover during the test sequence, for the specimen by Schoettler et al. [23]

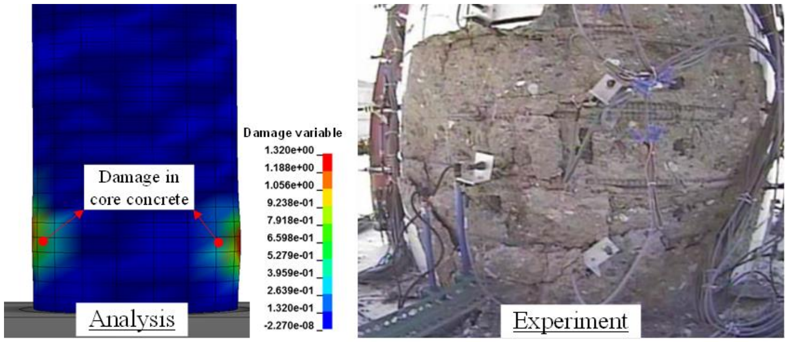

Fig. 11 – Damage at base of column specimen after the sixth motion (test picture taken from [23])

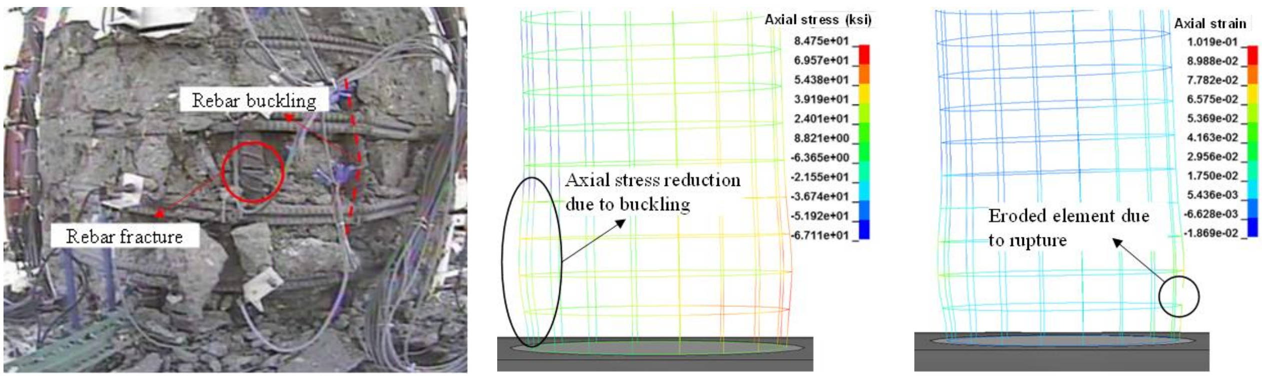

(a) Damage in test (picture from [23]) (b) Contours of axial stress (c) Contours of axial strain

Fig. 12 - Rebar buckling and first rebar fracture observed during the 8th motion, for the specimen tested by Schoettler at al. [23].

4. Conclusions

A novel triaxial constitutive model has been formulated and used for the analysis of reinforced concrete components and systems under cyclic loading. The model can capture all the significant aspects of material response under earthquake loads, such as the crack opening and closing and the increased material strength and ductility for confined compression. The model has been combined with a recently developed uniaxial stress-strain law for reinforcing steel and used in finite element analysis of components undergoing severe damage due to cover spalling, rebar buckling and subsequent rebar fracture. The analyses using the material model presented herein have been found capable of reproducing the global response and damage accumulation for experimentally tested specimens.

5. Acknowledgements

The authors wish to thank personnel of the Livermore Software and Technology Corporation (LSTC) for support in the implementation of the constitutive models in LS-DYNA. Furthermore, the support of the Advanced Research Computing (ARC) division of Virginia Tech for conducting the simulations in the cluster Blueridge is greatly appreciated. Finally, the authors wish to acknowledge the help of Professor K. Beyer and Dr. M. Schoettler in obtaining the recorded data from the experimental tests on the RC wall and the bridge pier, respectively. Any opinions expressed in this paper are those of the authors alone.

6. References

[1] Mander J, Priestley N, Park R (1988): Theoretical stress-strain model for confined concrete. *ASCE Journal of Structural Engineering*, **114** (8), 1804-1826.

[2] Imran I, Pantazopoulou S (2001): Plasticity model for concrete under triaxial compression. *ASCE Journal of Engineering Mechanics*, **127** (3), 281-290.

[3] Willam K, Warnke E (1974): Constitutive model for the triaxial behavior of concrete. *IABSE Report*, International Association of Bridge and Structural Engineers, **19**, 1-30.

[4] Ottosen N (1977): A failure criterion for concrete. *ASCE Journal of Engineering Mechanics*, **103**, 527-535.

[5] Hsieh S, Ting E, and Chen W (1982): A plastic fracture model for concrete. *International Journal of Solids and Structures*, **18** (3), 181-197.

[6] Selby R, Vecchio F. (1997): A Constitutive model for analysis of reinforced concrete solids. *Canadian Journal of Civil Engineering*, **24** (3), 460-470.

[7] Lee J, Fenves, G (1998): Plastic-damage model for cyclic loading of concrete structures. *ASCE Journal of Engineering Mechanics*, **124** (8), 892-900.

[8] Maekawa K, Pinanmas A, Okamura H (2003): *Nonlinear mechanics of reinforced concrete*. Spon Press.

[9] Grassl P, Jirasek M. (2006): Plastic model with non-local damage applied to concrete. *International Journal for Numerical and Analytical Methods in Geomechanics*, **30** (1), 71-90.

[10] Murray Y. (2007): User's manual for LS-DYNA material model 159. *Technical Report No. FHWA-HRT-05-062*, Federal Highway Administration, McLean, VA, USA.

[11] Caner F, Bažant Z (2012): Microplane model M7 for plain concrete. I: Formulation. *ASCE Journal of Engineering Mechanics*, **139** (12), 1714-1723.

[12] Moharrami M, Koutromanos I (2016): Triaxial constitutive model for concrete under cyclic loading. *ASCE Journal of Structural Engineering*, 10.1061/(ASCE)ST.1943-541X.0001491 , 04016039.

[13] Kang H, Willam K, Shing B, Spacone E. (2000): Failure analysis of R/C columns using a triaxial concrete model. *Computers & Structures*, **77** (5), 423-440.

[14] Lubliner J, Oliver J, Oller S, Onate E (1989): A plastic-damage model for concrete. *International Journal of Solids and Structures*, **25** (3), 299-326.

[15] Bažant Z (2002): Concrete fracture models: testing and practice. *Engineering fracture mechanics*, **69** (2), 165-205.

[16] Lu Y, Panagiotou M. (2013): Three-dimensional cyclic beam-truss model for nonplanar reinforced concrete walls. *ASCE Journal of Structural Engineering*, **140** (3), 0401307:1-11.

[17] Gopalaratnam V, & Shah S (1985): Softening response of plain concrete in direct tension. *ACI Journal proceedings*, **82** (3), 310-323.

[19] LSTC (2007): *LS-DYNA User's Manual*, Livermore Software and Technology Corporation, Livermore, CA, USA.

[19] Kim S, Koutromanos I (2016): Constitutive model for reinforcing steel under cyclic loading. *ASCE Journal of Structural Engineering*, accepted for publication.

[20] Dodd L, Restrepo-Posada J (1995): Model for predicting cyclic behavior of reinforcing steel. *ASCE Journal of Structural Engineering*, **121** (3), 433-445.

[21] Murcia-Delso J, Stavridis A, Shing P (2013): Bond Strength and Cyclic Bond Deterioration of Large-Diameter Bars. *ACI Structural Journal*, **110** (4), 659-670.

[22] Beyer K, Dazio A, Priestley N (2008): Quasi-static cyclic tests of two U-shaped reinforced concrete walls. *Journal of earthquake engineering*, **12** (7), 1023-1053.

[23] Schoettler M, Restrepo J, Guerrini G, Duck D, Carrea F (2015): A full-scale, single-column bridge bent tested by shake-table excitation. *Technical Report PEER 2015/02*, Pacific Earthquake Engineering Research Center, University of California, Berkeley, USA.